# Synergistic effects of magnesium ions and simvastatin on attenuation of high-fat diet-induced bone loss

Bingyang Dai [a],[1], Xu Li [a],[1], Jiankun Xu [a],[*], Yuwei Zhu [b], Le Huang [a], Wenxue Tong [a], Hao Yao [a], Dick Ho-kiu Chow [a], Ling Qin [a],[**]

[a] *Musculoskeletal Research Laboratory of Department of Orthopedics & Traumatology and Innovative Orthopaedic Biomaterial & Drug Translational Research Laboratory, Li Ka Shing Institute of Health Sciences, The Chinese University of Hong Kong, Hong Kong, China*
[b] *Department of Chemistry, The Chinese University of Hong Kong, New Territories, Hong Kong, China*

## ABSTRACT

*Introduction:* Magnesium (Mg) has a prophylactic potential against the onset of hyperlipidemia. Similar to statin, Mg is recommended as lipid-lowering medication for hypercholesterolemia and concomitantly exhibits an association with increased bone mass. The combination of statin with Mg ions ($Mg^{2+}$) may be able to alleviate the high-fat diet (HFD)-induced bone loss and reduce the side-effects of statin. This study aimed to explore the feasibility of combined $Mg^{2+}$ with simvastatin (SIM) for treating HFD-induced bone loss in mice and the involving mechanisms.

*Materials and methods:* C57BL/6 male mice were fed with a HFD or a normal-fat diet (NFD). Mice were intraperitoneally injected SIM and/or orally received water with additional $Mg^{2+}$ until sacrificed. Enzyme-linked immunosorbent assay was performed to measure cytokines and cholesterol in serum and liver lysates. Bone mineral density (BMD) and microarchitecture were assessed by micro-computed tomography (μCT) in different groups. The adipogenesis in palmitate pre-treated HepG2 cells were performed under various treatments.

*Results:* μCT analysis showed that the trabecular bone mass was significantly lower in the HFD-fed group than that in NFD-fed group since week 8. The cortical thickness in HFD-fed group had a significant decrease at week 24, as compared with NFD-fed group. The combination of $Mg^{2+}$ and SIM significantly attenuated the trabecular bone loss in HFD-fed mice via arresting the osteoclast formation and bone resorption. Besides, such combination also reduced the hepatocytic synthesis of cholesterol and inhibited *matrix metallopeptidase 13* (*Mmp13*) mRNA expression in pre-osteoclasts.

*Conclusions:* The combination of $Mg^{2+}$ and SIM shows a synergistic effect on attenuating the HFD-induced bone loss. Our current formulation may be a cost-effective alternative treatment to be indicated for obesity-related bone loss.

## 1. Introduction

Obesity is associated with increased risk of metabolic syndrome, including insulin resistance, abdominal obesity, hypertension, and dyslipidemia [1–3]. Epidemiological and pathophysiological evidences also show the link between osteoporosis and dyslipidemia, where the low bone mineral density (BMD) appears to be an indicator of cardiovascular mortality in obese individuals [4–6].

A high-cholesterol diet in rats shows a progressive osteopenic bone in line with increased serum osteocalcin and carboxyterminal collagen crosslinks [7]. Whereas, another *in vivo* study demonstrates that cholesterol potentiates osteogenic capacity of bone marrow mesenchymal stem cells (BMSCs) [8]. The explanation for this paradox is that the type of cholesterol (free cholesterol or cholesterol ester) is the major cause of the biological diversity on osteogenesis [8]. The elevation of free cholesterol concurrent low BMD conveys the negative effect of

hypercholesterolemia on the process of osteoporosis [8]. Thus, lowering the free cholesterol level in circulatory system may rescue the hypercholesterolemia induced bone metabolic disorders.

Statins are commonly recommended as lipid-lowering medications for hypercholesterolemia [9,10], and are also able to increase BMD [11, 12]. However, high dose of statins may lead to asymptomatic hepatotoxicity and serious muscle injury [13–15]. The risk of statin-induced newly diagnosed diabetes mellitus elevates about 0.2% per year [16]. Statins have an effect on risk reduction of atherothrombotic stroke and total stroke, but they possibly increase the risk of hemorrhagic stroke in patients with cerebrovascular diseases [17]. Statins competitively inhibit HMG-CoA reductase, the rate-limiting enzyme of the mevalonate pathway, inactivation of which requires the presence of magnesium ions ($Mg^{2+}$) [18,19]. In addition, $Mg^{2+}$ has a prophylactic potential against the onset of hyperlipidemia and cardiovascular diseases by reducing lipid indices [20]. In contrast, obesity-induced hyperglycemia could cause the hypomagnesemia in non-diabetic individuals [21–23]. Therefore, we formulated the notion that the combined supplementation of $Mg^{2+}$ with simvastatin (SIM) at a lower dose might synergistically reduce cholesterol synthesis, replenish the $Mg^{2+}$ scarcity in obese mice, and bypass the side-effects from statins treatment alone.

Bone remodeling requires the differentiation of BMSCs-derived osteoblasts along with subsequent collagen synthesis and the recruitment of hematopoietic-derived osteoclasts for bone resorption [24]. Still up for debate is the question on the explicit roles of $Mg^{2+}$ on bioactivities of the bone resident cells. Knockdown of $Mg^{2+}$ transporter SCL41A1 mitigates the inhibition of $Mg^{2+}$ for the osteogenic differentiation in BMSCs and promotes bone mineralization [25]. However, Mg-based implant exhibits biodegradability and osteo-inductive properties in our previous study [26]. $Mg^{2+}$ scarcity results in an increased formation of osteoclasts, but has no discernible effect on osteoclasts viability [27]. Whereas, the high levels of degradative products from Mg metal arrest the proliferation and mature differentiation of osteoclasts progenitors [28]. With regards to statins, the major mechanism on bone metabolism refers to promote osteogenesis by increasing viability and differentiation of osteoblasts [29], while inhibits osteoclastogenesis by impairing the prenylation of GTP-binding proteins [30]. No matter the direct regulation of bone resident cells activities or shrinkage the effects of hypercholesterolemia on these cells activities, $Mg^{2+}$ and SIM offer the possibility to alleviate the bone loss in high-fat diet (HFD)-fed mice.

Therefore, our overall hypothesis is that the combined supplementation of $Mg^{2+}$ and SIM could improve the lipid profiles in circulatory system while alleviates the bone loss in HFD-fed mice. Our findings confirmed that the combined therapy of $Mg^{2+}$ and SIM attenuated the HFD-induced bone loss via synergistically impaired osteoclast formation and activities, as well as limited the cholesterol synthesis.

## 2. Materials and methods

### 2.1. Animals

C57BL/6 mice (Twelve-week-old, male) were fed with a HFD (60% of total calories from fat, 20% from carbohydrate and 20% from protein, cat# D12492, Research Diets Inc.) [31]. The control group received a normal-fat diet (NFD; 10% of total calories from fat, 70% from carbohydrate and 20% from protein, cat# D12450J, Research Diets Inc.). Body weight was measured weekly. The mice in SIM group were intraperitoneally injected SIM 20 mg/kg/day until sacrificed [32,33]. The mice in Mg group were orally received water supplemented with $Mg^{2+}$ (magnesium chloride, 100 mg/kg/day) until sacrificed. The mice in the combination of $Mg^{2+}$ and SIM group were intraperitoneally injected SIM (20 mg/kg/day) and orally received $Mg^{2+}$ (100 mg/kg/day). The dosage was calculated based on the clinical trials on Mg supplementation (about 500 mg/day) in diseases with Mg deficiency [34–36]. If animals showed signs of suffering during the observation periods, they were humanely euthanized. All animals were housed under a 12-h light/dark cycle at the

Experimental Animal Center at the Prince of Wales Hospital and received NFD/HFD and water *ad libitum*. The specified experimental protocols were approved by the Animal Experiment Ethics Committee of the Chinese University of Hong Kong (17-184-MIS-5-C and 19-036-MIS-5-C).

### 2.2. Histological and histomorphometric analysis

After fixation in 4% paraformaldehyde (PFA) for 24 h, bone tissues were decalcified in 10% ethylene diamine tetraacetic acid (EDTA, pH 7.4, Sigma, cat# 798681) for 14 days, embedded in paraffin to prepare sections (5 μm thick) for routine staining [37].

Calcein green (10 mg/kg, Sigma, cat# C0875) and xylenol orange (90 mg/kg, Sigma, cat# 398187) were subcutaneously injected into the abdomen at day 10 and day 3 before sacrifice, respectively. After euthanasia, dehydrated tibiae were embedded in the methyl methacrylate (MMA, Sigma, cat# M55909) to prepare sections with 5 μm in thickness (Leica RM2255) along the sagittal plane. The mineral apposition rate (MAR, μm/day) and bone formation rate (BFR/BS, $\mu m^3/\mu m^2$/day) were calculated based on the fluorescence labeling of the proximal tibia under the growth plate [38]. Histomorphometric analysis was carried out using OsteoMeasure System (Osteometrics, Atlanta, GA, USA) according to a standard histomorphometry protocol [39].

### 2.3. Micro-computed tomography (μCT) imaging and analysis

Trabecular bone microstructure under the growth plate near the proximal tibia was reconstructed and analyzed, including about 1.5 mm length of bone mineral density (BMD), bone volume over total volume (BV/TV), trabecular thickness (Tb.Th), trabecular separation (Tb.Sp), and trabecular number (Tb.N) [40]. The microstructure of cortical bone at the femoral midshaft was reconstructed and analyzed, including 0.8 mm length of average cortical thickness (Ct.Th) and cortical porosity (Ct.Po) [40].

### 2.4. Isolation of bone marrow cells for mRNA analysis

Fresh bone marrow from proximal tibia was flushed out with phosphate-buffered saline (PBS) containing 1% fatty acid-free bovine serum albumin (BSA) and 1% RNase and DNase-free water using a 25-gauge needle [41]. Red blood cells were lysed using erythrocyte lysis buffer for 3 min at room temperature. After centrifugation at 1500 rpm for 5 min, cells were washed with PBS one time and added into Trizol reagent.

### 2.5. Isolation of bone marrow mesenchymal stem cells (BMSCs)

For BMSCs isolation, bone marrow cells from C57BL/6 mice (6-week-old, male) were flushed out with minimum essential medium (MEM, Gibco, cat# 61100061) [42]. The erythrocyte-deleted BMSCs were cultured in MEM supplemented with 15% fetal bovine serum (FBS, Gibco, cat# 16140071) and 1% Penicillin-Streptomycin-Neomycin (PSN, Gibco, cat# 15640055) and incubated at 37 °C with 5% $CO_2$. The medium was changed every 2 days. Cells were passaged until the 80% confluent. Immunofluorescent staining for stem cell surface markers (CD105 and CD44) in primary BMSCs and tri-lineage differentiations assays (adipogenesis, osteogenesis, and chondrogenesis) were performed.

### 2.6. Cell viability assay

The 3-(4,5-Dimethylthiazol-2-yl)-2,5-diphenyltetrazolium bromide (MTT, Invitrogen, cat# M6494) assay was performed to evaluate the effect of $Mg^{2+}$ (Sigma, cat# M8266) or SIM (Abcam, cat# ab120505) on the viability of BMSCs and bone marrow macrophages, respectively. For MTT test, the cells were seeded into 96-well plates at a density of 3 ×
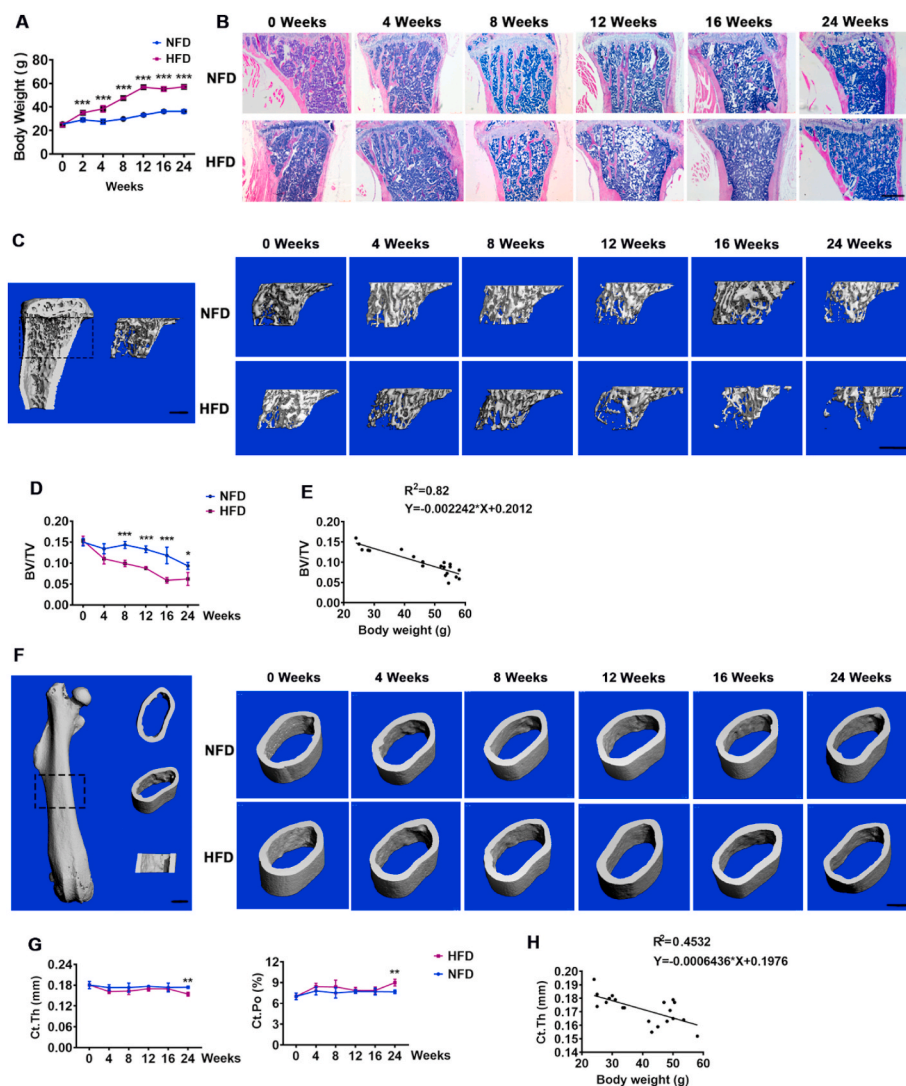
**Fig. 1.** HFD-fed group has a susceptibility to lower trabecular bone mass measured at proximal tibia as compared with that of NFD-fed group.

(A) Comparison of the body weights between NFD- and HFD-fed mice ($n = 5$). (B) Representative H&E staining of proximal tibiae from NFD- and HFD-fed mice at the indicated time points (Scale bar: 500 μm). (C, D) Representative μCT images and quantification ($n = 5$) of trabecular bone from standard region of interest (ROI) in proximal tibiae (Scale bar: 400 μm). (E) Linear regression analysis of the BV/TV of trabecular bone and body weight in HFD-fed mice within 24 weeks ($n = 20$). (F, G) Representative μCT images and quantification ($n = 5$) of cortical bone in the midshaft of femora (Scale bar: 400 μm). Ct.Th: cortical thickness; Ct.Po: cortical porosity. (H) Linear regression analysis of the Ct.Th of femur and body weight in HFD-fed mice within 24 weeks ($n = 20$). All data were presented as mean ± SD. $*P < 0.05$; $**P < 0.01$; $***P < 0.001$; by two-way ANOVA with *Sidak's post hoc* test (A, D, and G).

$10^3$ cells/well. After overnight incubation, the cells were treated with different concentrations of $Mg^{2+}$ or SIM for 0, 24, 48, and 72 h, respectively. At each time point, the cells were incubated with 50 μl (1 mg/ml) MTT solution at 37 °C for 4 h in dark. After discarding the MTT solution, 50 μl DMSO was added into each well, and the absorbance at 570 nm was detected.

### 2.7. Tri-lineage differentiation of BMSCs

BMSCs at passage 2 were exposed to $Mg^{2+}$ (0.8, 1.8, and 5 mM) or SIM (0, 0.1, 0.2, 0.5 and 1 μM) in osteogenic induction medium (low glucose DMEM medium containing 10% FBS, ascorbic acid (50 μg/ml, Sigma, cat# 795437), dexamethasone (10 nM, Sigma, cat# D1756), and β-glycerolphosphate (5 mM, Sigma, cat# 50020)). Medium was changed every 2 days. Cell lysates were homogenized for mRNA level analysis after induction for 3 days. Alkaline phosphatase (ALP, Sigma, cat# 86R-1 KT) staining was performed after induction for 6 days. Alizarin Red S (Sigma, cat# 130-22-3) staining was performed after induction for 10 days.

Besides, BMSCs at passage 2 were exposed to $Mg^{2+}$ (0.8, 1.8, and 5 mM) or SIM (0, 0.1, 0.2, 0.5 and 1 μM) under adipogenic induction medium (high glucose DMEM medium containing 10% FBS, 3-isobutyl-1-methylxanthine (0.5 mM, IBMX, Sigma, cat# I7018), insulin (5 μg/ml, Sigma, cat# I2643), indomethacin (50 μM, Sigma, cat# I7378), and dexamethasone (500 nM)). The mRNA expression level was analyzed

after induction for 3 days. Oil red O (Sigma, cat# O0625) staining was performed for lipid droplet formation after induction for 7 days.

BMSCs at passage 2 ($5 \times 10^5$ cells) were centrifuged to a pellet at 1200 rpm for 5 min using centrifuge tubes and then cultured in chondrogenic induction medium (high glucose DMEM medium containing 10% FBS, 1% PSN, TGF-β3 (10 ng/ml), BMP-2 (500 ng/ml), dexamethasone (100 nM), and ascorbate-2-phosphate (50 μg/ml)) at 37 °C incubator with 5% $CO_2$. The medium was carefully replaced with fresh induction medium every 2 days. Fast green and safranin O staining was performed to evaluate the chondrogenesis after induction for 21 days [43].

### 2.8. Bone marrow-derived macrophages (BMDMs) and osteoclastogenic differentiation

For isolation of BMDMs, the bone marrow from C57BL/6 mouse (6-week-old, male) was flushed out with MEM and plated in MEM containing 10% FBS and 1% PSN. Non-adherent cells were collected after 12 h, and the erythrocyte-deleted cell pellet was resuspended in DMEM/F12 (Gibco, cat# 10565018) medium containing 10% FBS, 1% PSN, and macrophage colony-stimulating factor (M-CSF, 30 ng/ml, Gibco, cat# PHG6054).

BMDMs at passage 1 were cultured in DMEM/F12 medium containing 10% FBS, 1% PSN, M-CSF (30 ng/ml), and RANK ligand recombinant human protein (RANKL, 30 ng/ml, Gibco, cat# PHP0034) for
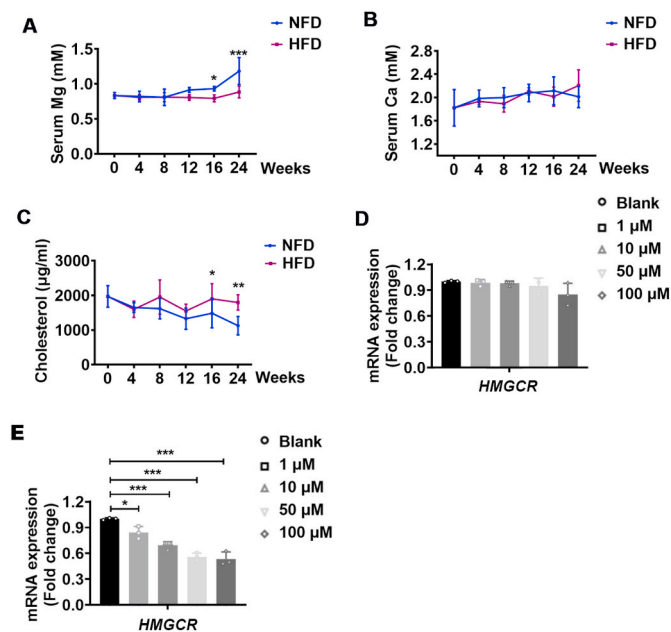
**Fig. 2.** The alterations of $Mg^{2+}$, $Ca^{2+}$, and cholesterol levels in serum. (A) Comparison of the concentrations of serum $Mg^{2+}$ between NFD- and HFD-fed mice ($n = 6$). (B) Comparison of the concentrations of serum $Ca^{2+}$ between NFD- and HFD-fed mice ($n = 6$). (C) Comparison of the concentrations of serum cholesterol between NFD- and HFD-fed mice ($n = 5$). (D) Relative expression of *3-hydroxy-3-methylglutaryl-CoA reductase* (*HMGCR*) in HepG2 cells treated with different concentrations of nitrendipine (an inhibitor of $Mg^{2+}$ channel) for 2 days ($n = 3$). (E) Relative expression of *HMGCR* in HepG2 cells treated with different concentrations of BAY K8644 (an agonist of $Mg^{2+}$ channel) for 2 days ($n = 3$). All data were presented as mean $\pm$ SD. *$P < 0.05$; **$P < 0.01$; ***$P < 0.001$; by two-way ANOVA with *Sidak's post hoc* test (A, B, and C), by one-way ANOVA with *Tukey's post hoc* test (D and E).

2 days to generate pre-osteoclasts and above 5 days to generate multi-nucleated mature osteoclasts [44].

### 2.9. Fatty acid treatment

HepG2 cells, a human hepatoma cell line (American Type Culture Collection, Rockville, MD, USA), were grown in high-glucose DMEM at 37 °C containing 10% FBS, 1% PSN. Palmitic acid powder (Sigma, cat# P9767) was added to a 10% solution of fatty acid free BSA and dissolved by shaking gently overnight at 37 °C to yield the stock solution (8 mM). The final molar ratio of free fatty acid to BSA was 5.2:1 [45]. Sub-confluent monolayer HepG2 cells were pre-treated with or without Mg, SIM, or Mg + SIM for 24 h, and then stimulated with or without palmitic acid (0.4 mM) for another 24 h. BSA (0.5%, w/v) was added in the control group. Cells were stained with BODIPY (Invitrogen, cat# D3922) to examine the amount of neutral lipid accumulation in HepG2 cells.

### 2.10. Serum measurements

Blood samples were collected before mice euthanasia. After clotting and centrifuging, serum was collected and stored at −80 °C until assayed. Cholesterol (Abcam, cat# ab65390), procollagen type I N-terminal propeptide (P1NP, Abclonal, cat# RK03119), C-terminal telopeptide of type I collagen (CTX1, Abclonal, cat# EMC0850), high-density lipoprotein (HDL, Abcam, cat# ab65390), low-density lipoprotein (LDL, Abcam, cat# ab65390) and very low-density lipoprotein (VLDL, Abcam, cat# ab65390) in serum were measured as manufacturer's instructions. The concentrations of $Mg^{2+}$ and Ca ion ($Ca^{2+}$) in serum were measured using inductively coupled plasma optical

emission spectroscopy (ICP-OES, Shimadzu Europa Gmbh, Germany) at 280 nm and 318 nm absorbances, respectively [46].

### 2.11. Liver lysates for cholesterol measurements

For analysis of liver lipid content, frozen liver tissue (20 mg) was homogenized in cholesterol assay buffer (100 µl, Abcam, cat# ab65390) on ice. Collection of the supernatant was regarded as total cholesterol after centrifugation for 8 min at 4 °C and 13,000 rpm. After incubation of mixture of sample (100 µl, above supernatant) with 2X Precipitation Buffer (100 µl) for 10 min at room temperature, the supernatant was collected as HDL fraction after centrifugation for 10 min at 2000 g. The resuspended precipitation in PBS (200 µl) was regarded as LDL/VLDL fraction.

### 2.12. Cholesterol solution

To yield the stock solution (12.5 mg/ml) of cholesterol (Sigma, cat# C8667), we added cholesterol (25 mg) in absolute ethyl alcohol (2 ml) and incubated at 75 °C with gentle vibration until dissolved.

### 2.13. Mechanical testing

Three-point bending strength was performed using a mechanical testing machine (H25KS Hounsfield Test Equipment, Redhill, Surrey, UK). The femur (with the anterior surface upwards) was positioned horizontally on the two holding pivots setting with a constant span length of 10 mm. The pressing force was vertically directed to the femoral midshaft. Each bone was compressed with a constant speed of 5 mm/min until failure. Breaking force was defined as failure load. Stiffness was calculated by the slope of the linear (elastic) part of the load-displacement curve [47].

### 2.14. Quantitative real-time polymerase chain reaction (qRT-PCR)

Total RNA was extracted using Trizol reagent. RNA was quantified spectrophotometrically based on the A260 using a ND-1000 spectrophotometer (NanoDrop Technologies, Wilmington, DE, USA). mRNA was reversely transcribed to cDNA using the cDNA kit (Takara). cDNA was amplified in a mixture reaction system containing SYBR Green qPCR SuperMix-UDG (Takara) and specific primer sequences (Table S1) [48]. qRT-PCR analysis was performed using ABI 7900HT platform (Applied Biosystems, Waltham, MA, USA).

### 2.15. Statistical analysis

All the mice were randomly assigned to the indicated groups. The performances such as the distributions, treatments, and assessments were not blinded, but the results were confirmed by three independent investigators. Statistical analyses were performed using one-way ANOVA with *Tukey's post hoc* test for comparison of control/normal and other treatment groups or two-way ANOVA with *Sidak's post hoc* test for among-group comparisons (with the purpose to determine if there is synergistic effect). Numerical values for each measurement were displayed as mean $\pm$ standard deviation (SD). $P < 0.05$ was defined as statistical significance. GraphPad Prism (version 8.2.1) was used for all statistical analysis.

## 3. Results

### 3.1. HFD-fed group has a susceptibility to lower trabecular bone mass measured at proximal tibia as compared with that of NFD-fed group

The body weights began to diverge at week 2 of the HFD-fed group showing a significantly greater body weight than that of NFD-fed group (Fig. 1A). µCT and histological analysis of the trabecular bone showed
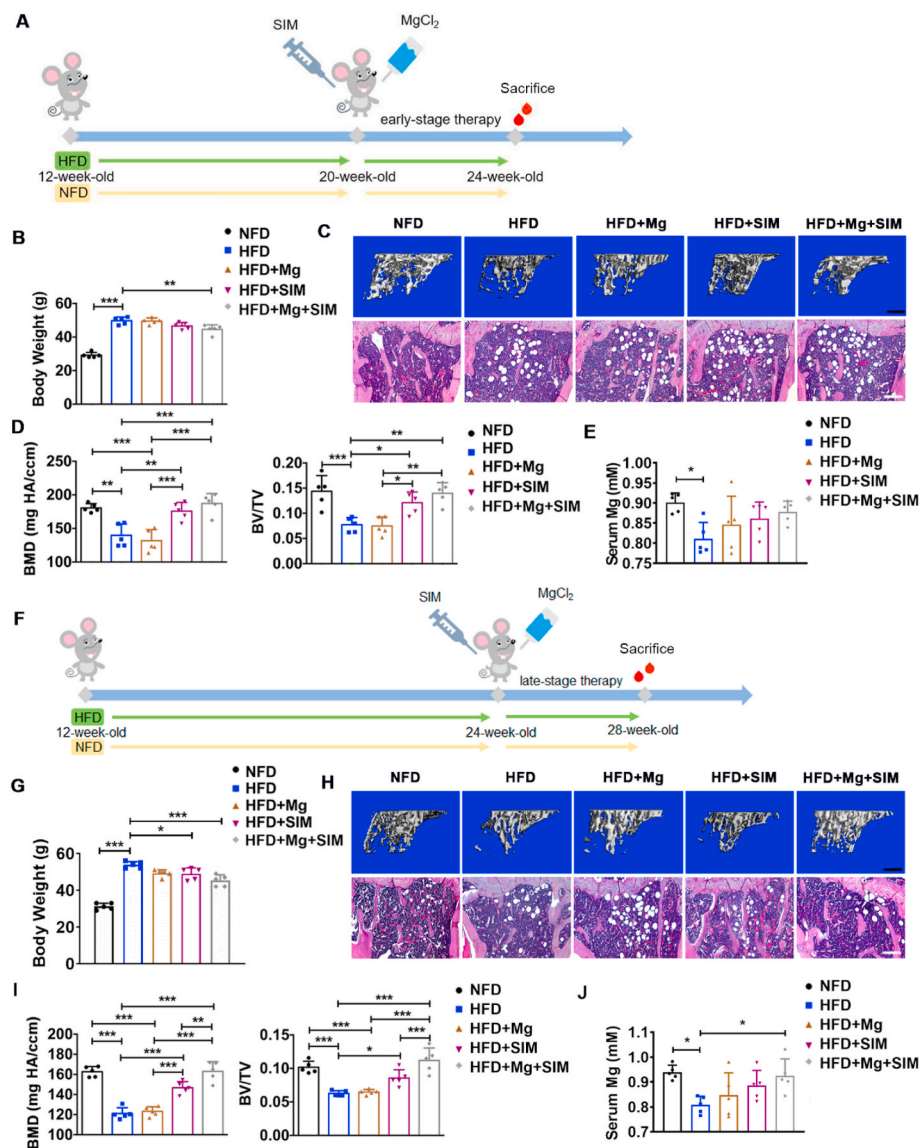
**Fig. 3.** Combination of $Mg^{2+}$ and SIM attenuates the trabecular bone loss in HFD-fed mice.
(A) Schematic diagram illustrating the early-stage therapy. (B) Comparison of the body weights between NFD, HFD, HFD + Mg, HFD + SIM, and HFD + Mg + SIM groups at the early-stage therapy (at week 8 post HFD-feeding, the mice were received treatment for another 4 weeks) ($n = 5$). (C) Representative μCT images and H&E staining of proximal tibiae at the early-stage therapy (Scale bar: 400 μm). (D) Quantification of trabecular bone from standard ROI in proximal tibiae at the early-stage therapy ($n = 5$). (E) Comparison of the concentrations of serum $Mg^{2+}$ at the early-stage therapy ($n = 5$). (F) Schematic diagram illustrating the late-stage therapy. (G) Comparison of the body weights between NFD, HFD + Mg, HFD + SIM, and HFD + Mg + SIM groups at the late-stage therapy (at week 12 post HFD-feeding, the mice were received treatment for another 4 weeks) ($n = 5$). (H) Representative μCT images and H&E staining of proximal tibiae at the late-stage therapy (Scale bar, 400 μm). (I) Quantification of trabecular bone from standard ROI in proximal tibiae at the late-stage therapy ($n = 5$). (J) Comparison of the concentrations of serum $Mg^{2+}$ at the late-stage therapy ($n = 5$). All data were presented as mean ± SD. *$P < 0.05$; **$P < 0.01$; ***$P < 0.001$; by one-way ANOVA with *Tukey's post hoc* test (B and G), by two-way ANOVA with *Sidak's post hoc* test (D, E, I, and J).

that BV/TV in the HFD-fed group was significantly lower than that in the NFD-fed group after week 8 (Fig. 1B–D). Linear regression analysis showed that the body weight was negatively correlated with BV/TV under HFD-fed group (Fig. 1E). μCT analysis of the cortical bone at the femoral midshaft showed a significantly lower value of cortical thickness and a significantly higher cortical porosity in the HFD-fed group than that in the NFD-fed group at the week 24 (Fig. 1F and G). Linear regression analysis showed that body weight was negatively correlated with cortical thickness in mice with HFD-fed (Fig. 1H). These results demonstrate that HFD-fed group has a susceptibility to lower trabecular bone mass measured at proximal tibia as compared with that of NFD-fed group.

### 3.2. Combination of $Mg^{2+}$ and SIM attenuates the trabecular bone loss in HFD-fed mice

The concentration of serum $Mg^{2+}$ in the HFD-fed group showed a significantly lower level than that of the NFD-fed group since week 16 (Fig. 2A). Rather, the concentration of serum $Ca^{2+}$ in HFD-fed group was similar to that in NFD-fed group (Fig. 2B). In line with what we mentioned previously, obesity-induced hyperglycemia was the cause of hypomagnesemia [23]. The concentration of serum cholesterol was

higher in the HFD-fed group than that in the NFD-fed group since week 16 as well, indicating a potential relationship between serum $Mg^{2+}$ and cholesterol (Fig. 2C). Nitrendipine, the $Mg^{2+}$ channel antagonist, did not affect the gene expression of *3-hydroxy-3-methylglutaryl-CoA reductase* (*HMGCR*) in HepG2 cells (a commonly used human liver cancer cell line) *in vitro* (Fig. 2D). While BAY K8644, the $Mg^{2+}$ channel agonist, significantly inhibited the gene expression of *HMGCR* in HepG2 cells (Fig. 2E). These results suggest that the HMG-CoA reductase synthesis could be affected by the concentration of $Mg^{2+}$ in hepatocyte where the cholesterol is produced.

Based on the individual variation of trabecular bone mass, we defined two stages of HFD-induced bone loss: early stage ranged from week 8 to week 12, and late stage started from week 12 to week 16. In order to perform the early-stage therapy, at week 8 post HFD-feeding, the mice were treated with $Mg^{2+}$ and/or SIM for another 4 weeks (Fig. 3A). The body weight of combination of $Mg^{2+}$ and SIM group (combined group) was significantly lower than that of the HFD-fed group (Fig. 3B). Both BMD and BV/TV of proximal tibia in the combined group were significantly higher than that in the HFD-fed group (Fig. 3C and D). Although the concentration of serum $Mg^{2+}$ in combined group was slightly higher than that in the HFD-fed group, combined treatment could not normalize the concentration of serum $Mg^{2+}$ in early-
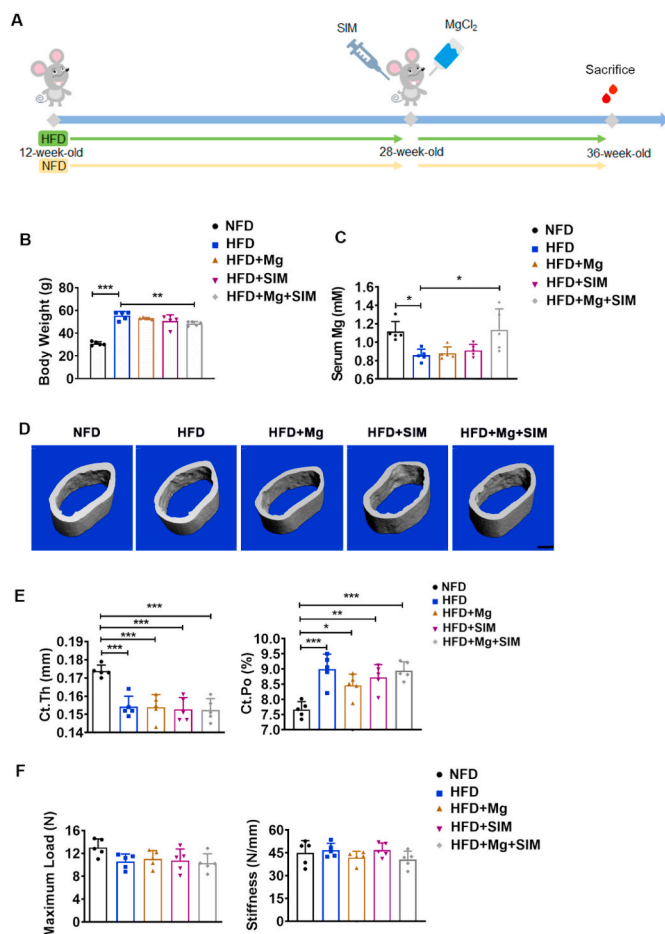
**Fig. 4.** Combination of $Mg^{2+}$ and SIM fails to attenuate the cortical bone loss in HFD-fed mice.
(A) Schematic diagram illustrating the combination of $Mg^{2+}$ and SIM to prevent the cortical bone mass loss. (B) Comparison of the body weights among NFD, HFD, HFD + Mg, HFD + SIM, and HFD + Mg + SIM groups (at week 16 post HFD-feeding, the mice were received treatment for another 8 weeks, $n = 5$). (C) Comparison of the concentrations of serum $Mg^{2+}$ in the NFD, HFD, HFD + Mg, HFD + SIM, and HFD + Mg + SIM groups (at week 16 post HFD-feeding, the mice were received treatment for another 8 weeks, $n = 5$). (D, E) Representative μCT images and quantification ($n = 5$) of cortical bone mass at the femoral midshaft (Scale bar: 400 μm). (F) Maximum load and stiffness at the femoral midshaft ($n = 5$). All data were presented as mean ± SD. *$P < 0.05$; **$P < 0.01$; ***$P < 0.001$; by one-way ANOVA with *Tukey's post hoc* test (B and F), by two-way ANOVA with *Sidak's post hoc* test (C and E).

stage therapy (Fig. 3E). In order to perform the late-stage therapy, at week 12 post HFD-feeding, the mice were treated with $Mg^{2+}$ and/or SIM for another 4 weeks (Fig. 3F). The body weight of the combined group was significantly lower than that of the HFD-fed group (Fig. 3G). Both BMD and BV/TV of the combined group were substantially higher than that of the HFD-fed group (Fig. 3H and I). The concentration of serum $Mg^{2+}$ in combined group was substantially greater than that in HFD-fed group (Fig. 3J).

To prevent cortical bone loss, at week 16 post HFD-feeding, the mice were treated with $Mg^{2+}$ and/or SIM for another 8 weeks (Fig. 4A). The body weight of the combined group was significantly lower than that of the HFD-fed group (Fig. 4B). The concentration of serum $Mg^{2+}$ in the combined group was substantially greater than that in HFD-fed group (Fig. 4C). However, the cortical thickness and porosity of the combined group were similar to the HFD-fed group, indicating that the combination of $Mg^{2+}$ and SIM supplement had no synergistic effect on cortical bone mass in HFD-fed mice (Fig. 4D and E). The three-point bending

biomechanical test also confirmed such finding with no significant difference found in the maximum load and stiffness between the combined treatment group and HFD-fed group (Fig. 4F). These results demonstrate that the combination of $Mg^{2+}$ and SIM leads to a synergistic effect on prevention of trabecular bone loss but fails to rescue the cortical bone loss in our designed experiments.

### 3.3. The combination of $Mg^{2+}$ and SIM arrests the osteoclast formation and bone resorption when starting treatment at the late stage of bone loss

To avoid the skeletal adaption to the changes of body weight, we thus explored the mechanism of combined therapy of bone loss based on the steady body weight at the late-stage therapy. Due to large individual variation of trabecular mass between NFD- and HFD-fed mice, the levels of bone resorption marker, CTX1, and bone formation marker, P1NP, could not clearly reflect the activities or numbers of osteoblasts and osteoclasts at the late stage (Fig. 5A). An apposition rate represents the activity of a group of osteoblasts, and a formation rate is determined by the remodeling activation and the number of osteoblast [39]. The double labeling of calcein green and xylenol orange suggested the similar new-bone formation in the different treatment groups as compared with the HFD-fed group (Fig. 5B and C). The histomorphometric analysis showed similar osteoblast number and significantly decreased osteoclast number in proximal tibiae of combined group as compared with the HFD group (Fig. 5D and E). The expression level of bone formation marker Runt-related transcription factor 2 (RUNX2) was similar between the combined group and the HFD-fed group (Fig. 5F). However, the expression level of bone resorption marker Cathepsin K (CTSK) in the combined group was significantly lower than that in the HFD group (Fig. 5G). These results suggest that combination of $Mg^{2+}$ and SIM may attenuate the HFD-induced bone loss through inhibiting the osteoclast formation and bone resorption.

### 3.4. $Mg^{2+}$ and SIM play roles in the bone marrow cells differentiation

We isolated the mouse BMSCs that positively expressed stem cell markers and possessed tri-lineage differentiation capacities (adipogenesis, osteogenesis, and chondrogenesis) (Figs. S1A–D). MTT assay showed that high dose of $Mg^{2+}$ (higher than 5 mM) or SIM (higher than 1 μM) exerted cytotoxicity (decreased the cellular metabolic activity by the value of half maximal inhibitory concentration) to BMSCs, as well as BMDMs (Figs. S1E–H).

ALP activity, mineralized nodule formation, and osteogenic mRNA expression in the groups of $Mg^{2+}$ supplementation (1.8 mM and 5.0 mM) were similar to the group without $Mg^{2+}$ treatment (0.8 mM) under osteogenic induction (Fig. 6A and B). Besides, $Mg^{2+}$ supplementation at tested concentrations did not show effect on adipogenesis and osteoclastogenesis as compared with the group without $Mg^{2+}$ treatment (0.8 mM) (Fig. 6A and 6C-E).

Although SIM did not diverge the process of osteogenesis or adipogenesis of BMSCs (Fig. 6F–H), it could significantly arrest the process of osteoclastogenesis and the synthesis of bone matrix degrading enzyme, except for the significantly increased *matrix metallopeptidase 13* (*Mmp13*) with 1 μM SIM intervention (Fig. 6F and 6I-J). We subsequently combined a low dose of SIM (0.5 μM) with different concentrations of $Mg^{2+}$ (0.8, 1.8, and 5 mM) *in vitro*. The combined application had an inhibitory effect on the mRNA expression of *Mmp2* and *Mmp13* in pre-osteoclasts (Fig. 6K-M). These findings suggest that SIM substantially inhibits the process of osteoclastogensis and the synthesis of bone matrix degrading enzyme (*Ctsk* and *Mmp9*), while the combination of $Mg^{2+}$ with a low dose of SIM further dampens the bone matrix degrading enzyme (*Mmp2* and *Mmp13*) *in vitro*.

### 3.5. Cholesterol activates the Mmp13 expression in pre-osteoclasts

Histomorphometric analysis revealed a significant increased number
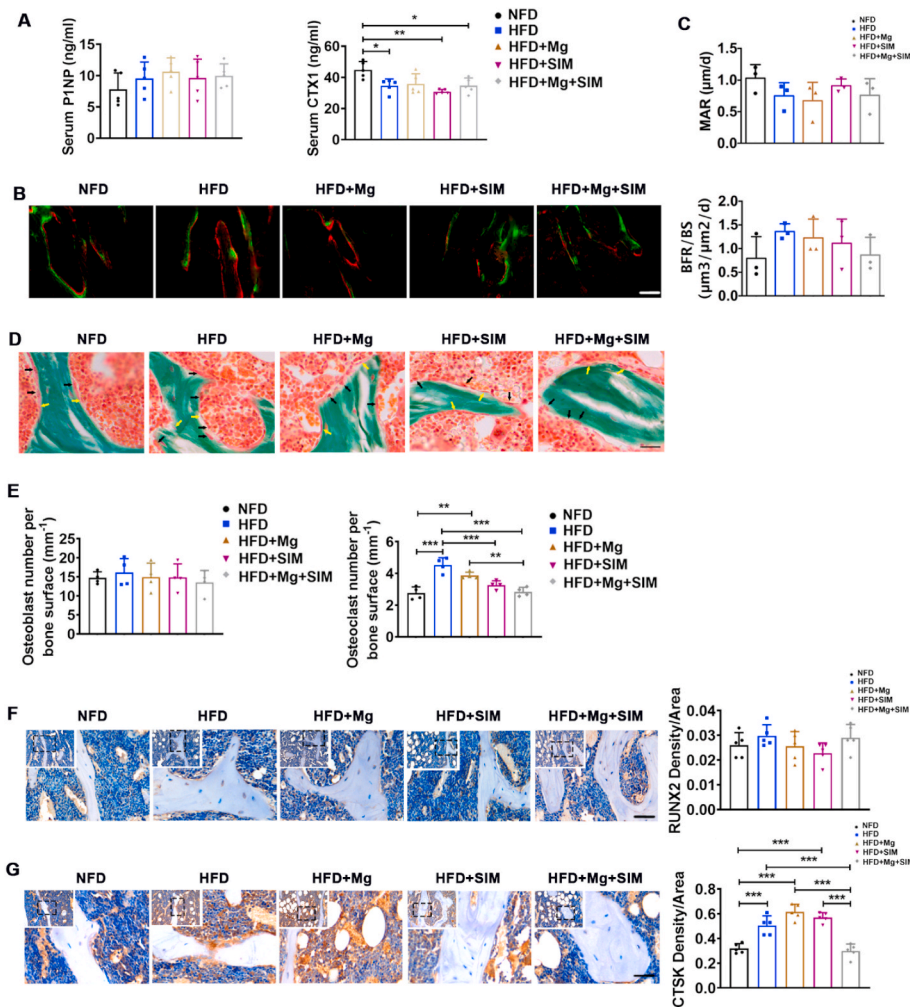
**Fig. 5.** Combination of $Mg^{2+}$ and SIM decreases the osteoclasts number and activity in HFD-fed mice at the late-stage therapy.

(A) Bone formation marker of procollagen type I N-terminal propeptide (P1NP) and bone resorption marker of C-terminal telopeptide of type I collagen (CTX1) in serum of the NFD, HFD, HFD + Mg, HFD + SIM, and HFD + Mg + SIM groups at the late-stage therapy ($n = 5$). (B, C) Representative calcein green and xylenol orange images and quantification of bone remodeling in proximal tibiae of the NFD, HFD, HFD + Mg, HFD + SIM, and HFD + Mg + SIM groups at the late-stage therapy ($n = 3$, Scale bar: 100 μm). (D, E) Representative Goldner's trichrome staining and quantification of osteoblast/osteoclast number on the surface ($n = 4$) of trabecular bone in proximal tibiae of the NFD, HFD, HFD + Mg, HFD + SIM, and HFD + Mg + SIM groups at the late-stage therapy (Scale bar: 25 μm; osteoclasts, black arrows; osteoblasts, yellow arrows). (F) Representative images and quantification of immunohistochemical stained RUNX2-positive cells in proximal tibiae at the late-stage therapy ($n = 5$, Scale bar: 50 μm). (G) Representative images and quantification of immunohistochemical stained CTSK-positive cells in proximal tibiae at the late-stage therapy ($n = 5$, Scale bar: 50 μm). All data were presented as mean ± SD. *$P < 0.05$; **$P < 0.01$; ***$P < 0.001$; by two-way ANOVA with *Sidak's post hoc* test (A, C, E, F, and G).

of osteoclasts in the HFD-fed group. Then we incubated pre-osteoclasts with different concentrations of cholesterol under osteoclastogenic induction condition. The high concentration of cholesterol (50 μg/ml) activated the expression of *Mmp13* without affecting other genes expression, such as *Ctsk, Nuclear factor of activated T-cells, cytoplasmic 1 (Nfatc1), Mmp2*, and *Mmp9* (Figs. 7A and S2A). However, the combination of $Mg^{2+}$ and SIM could not directly arrest the gene expression of *Mmp13* in cholesterol-treated pre-osteoclasts *in vitro* (Figs. 7B and S2B).

### 3.6. The combination of $Mg^{2+}$ and SIM reduces the synthesis of cholesterol in hepatocytes of HFD-fed mice

The combined utilization of $Mg^{2+}$ and SIM might produce synergistic effects on lowering cholesterol, while replenished the $Mg^{2+}$ for HFD-fed mice that mostly occurred the hypomagnesemia. We found that the cholesterol level in serum of combined group was significantly lower than that of HFD-fed group for the late-stage therapy (Fig. 7C). The high-density lipoprotein (HDL) transports cholesterol mostly to the liver or steroidogenic organs such as adrenals and ovary [49]. Low-density lipoprotein (LDL) and very low-density lipoprotein (VLDL) released from the liver delivers carried fat molecules to cells (adipose, cardiac muscle, and skeletal muscle) [50]. We found that the HDL and LDL/VLDL levels were similar between combined group and HFD-fed group in the late-stage therapy (Fig. 7D and E).

Therefore, we speculated that the decreased level of cholesterol in serum was correlated with the compromised cholesterol synthesis in liver instead of the alteration of lipid transportation. Quantification of

the lipid-containing area in liver sections demonstrated that the combination of $Mg^{2+}$ and SIM substantially reduced the accumulation of lipid in liver from HFD-fed mice at both early and late stage (Fig. 7F–G and S3A-B). Meanwhile, the cholesterol level of liver lysate in the combined group was significantly less than that in HFD-fed group (Fig. 7H). Moreover, the adipogenesis was substantially inhibited by the combination of $Mg^{2+}$ and SIM in palmitate pre-treated HepG2 cells, which imitated the micro-milieu of cholesterol synthesis *in vitro* (Fig. 7I and J). Therefore, the combination of $Mg^{2+}$ and SIM reduces the hepatocytic synthesis of cholesterol *in vivo* and *in vitro*.

### 4. Discussion

SIM is widely used for preventing cardiovascular diseases. SIM also exerts positive biologic effects on bone formation partially via competitively binding HMG-CoA reductase, whose inactivation requires the participation of $Mg^{2+}$ [51]. However, the possibility of the combination of $Mg^{2+}$ and SIM in preventing bone loss remains elusive. As summarized in Fig. 8, our results corroborate for the first time that the combination of $Mg^{2+}$ and SIM leads to synergistic effects on the attenuating HFD-induced bone loss via impairing the osteoclast maturation and bone resorption. The combination could directly limit the hepatocytic synthesis of cholesterol and inhibits *Mmp13* mRNA expression in pre-osteoclasts.

Recent clinical studies demonstrate that body weight *per se* negatively correlates with bone mass when the effect of gravity is eliminated [52–54]. Growing epidemiological evidences, as well as animal studies,
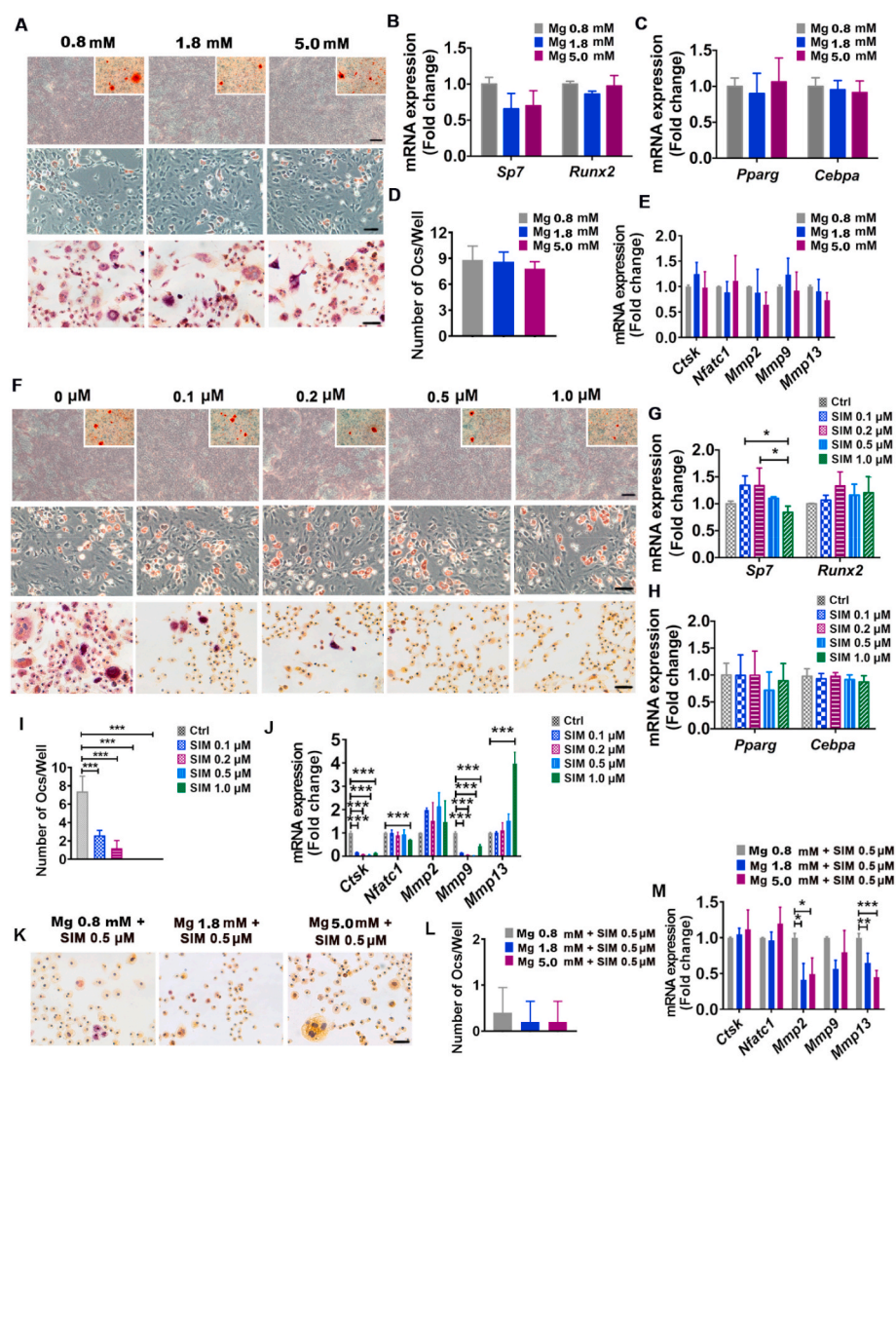
**Fig. 6.** Combination of Mg$^{2+}$ and SIM arrests the osteoclast formation and activities *in vitro*.
(A) Representative images of ALP staining (top, BMSCs after osteogenic induction for 6 days (Scale bar: 250 μm). The top right corner is the representative images of Alizarin Red S staining.), Oil red O staining (middle, BMSCs after adipogenic induction for 7 days, Scale bar: 100 μm), and TRAP staining (bottom, BMDMs after osteoclastogenic induction for 7 days, Scale bar: 50 μm) under different concentrations of Mg$^{2+}$. (B) Relative expression of *Sp7* and *Runx2* in BMSCs after osteogenic induction for 3 days under different concentrations of Mg$^{2+}$ ($n = 3$). (C) Relative expression of *Pparg* and *Cebpa* in BMSCs after adipogenic induction for 3 days under different concentrations of Mg$^{2+}$ ($n = 3$). (D) Quantification ($n = 5$) of Trap + osteoclast number in BMDMs after osteoclastogenic induction for 7 days under different concentrations of Mg$^{2+}$. (E) Relative expression of *Ctsk, Nuclear factor of activated T-cells, cytoplasmic 1* (*Nfatc1*), *matrix metallopeptidase 2* (*Mmp2*), *Mmp9*, and *Mmp13* in BMDMs after osteoclastogenic induction for 3 days under different concentrations of Mg$^{2+}$ ($n = 3$). (F) Representative images of ALP staining (top, BMSCs after osteogenic induction for 6 days (Scale bar: 250 μm). The top right corner is the representative images of Alizarin Red S staining.), Oil red O staining (middle, BMSCs after adipogenic induction for 7 days (Scale bar: 100 μm), and TRAP staining (bottom, BMDMs after osteoclastogenic induction for 7 days (Scale bar: 50 μm) under different concentrations of SIM. (G) Relative expression of *Sp7* and *Runx2* in BMSCs after osteogenic induction for 3 days under different concentrations of SIM ($n = 3$). (H) Relative expression of *Pparg* and *Cebpa* in BMSCs after adipogenic induction for 3 days under different concentrations of SIM ($n = 3$). (I) Quantification of Trap + osteoclast number in BMDMs after osteoclastogenic induction for 7 days under different concentrations of SIM ($n = 5$). (J) Relative expression of *Ctsk, Nfatc1, Mmp2, Mmp9,* and *Mmp13* in BMDMs after osteoclastogenic induction for 3 days under different concentrations of SIM ($n = 3$). (K, L) Representative images of TRAP staining and quantification ($n = 5$) of Trap + osteoclast number in BMDMs after osteoclastogenic induction for 7 days (Scale bar: 50 μm). (M) Relative expression of *Ctsk, Nfatc1, Mmp2, Mmp9,* and *Mmp13* in BMDMs after osteoclastogenic induction for 3 days with indicated treatments ($n = 3$). All data were presented as mean ± SD. *$P < 0.05$; **$P < 0.01$; ***$P < 0.001$; by one-way ANOVA with *Tukey's post hoc* test (B, C, D, E, G, H, I, J, L, and M).

offer an explanation that the metabolic syndrome in abdominal obesity is responsible for the bone loss [55–57]. Indeed, a mouse strain (C57BL/6) with a susceptibility to atherosclerosis is prone to bone loss in response to a HFD than atherosclerosis-resistant strains [58].

All statins possess a structural component that is extremely similar to the HMG portion of HMG-CoA, and statins sterically shield substrate binding by integrating to the active site of HMG-CoA reductase. In fact, Mg$^{2+}$ is also another regulator for the deactivated HMG-CoA reductase [18,59], which is the fourth abundant element in the body and the second abundant in the intracellular compartment [35]. Mg$^{2+}$ is a cofactor in more than 300 enzymatic reactions and critically stabilizes enzymes, including many adenosine triphosphate (ATP)-generating reactions. Moreover, Mg$^{2+}$ is universally required for the ATP-consumption reactions of glucose utilization, synthesis of fat, proteins, nucleic acids and coenzymes, muscle contraction, methyl group transfer and many other processes [60,61]. At least two

Mg$^{2+}$-dependent reactions are required to deactivate HMG-CoA Reductase [18,36]. The effect of the systemic administration of statins is limited due to its metabolism in the liver and clearance from first-pass elimination. In addition, high-dose administration of SIM is reported to cause severe adverse sides [62]. Previous study suggests that Mg$^{2+}$ supplementation could increase the SIM passive diffusion in hepatocytes and its pharmacological actions on cholesterol biosynthesis [63]. Low dietary Mg intake and hypomagnesemia are strongly associated with increased risk of developing lipid metabolic disorders [64,65]. In addition, because obesity is usually related with hypomagnesemia, it has been suggested that obesity deteriorates the Mg status [66]. However, the regression analysis shows no correlation between body weight status and the hypomagnesemia, indicating that hypomagnesemia is an epiphenomenon related with obesity rather than the causal relationship between body weight.

Low-density lipoprotein (LDL) is the major source of transferred
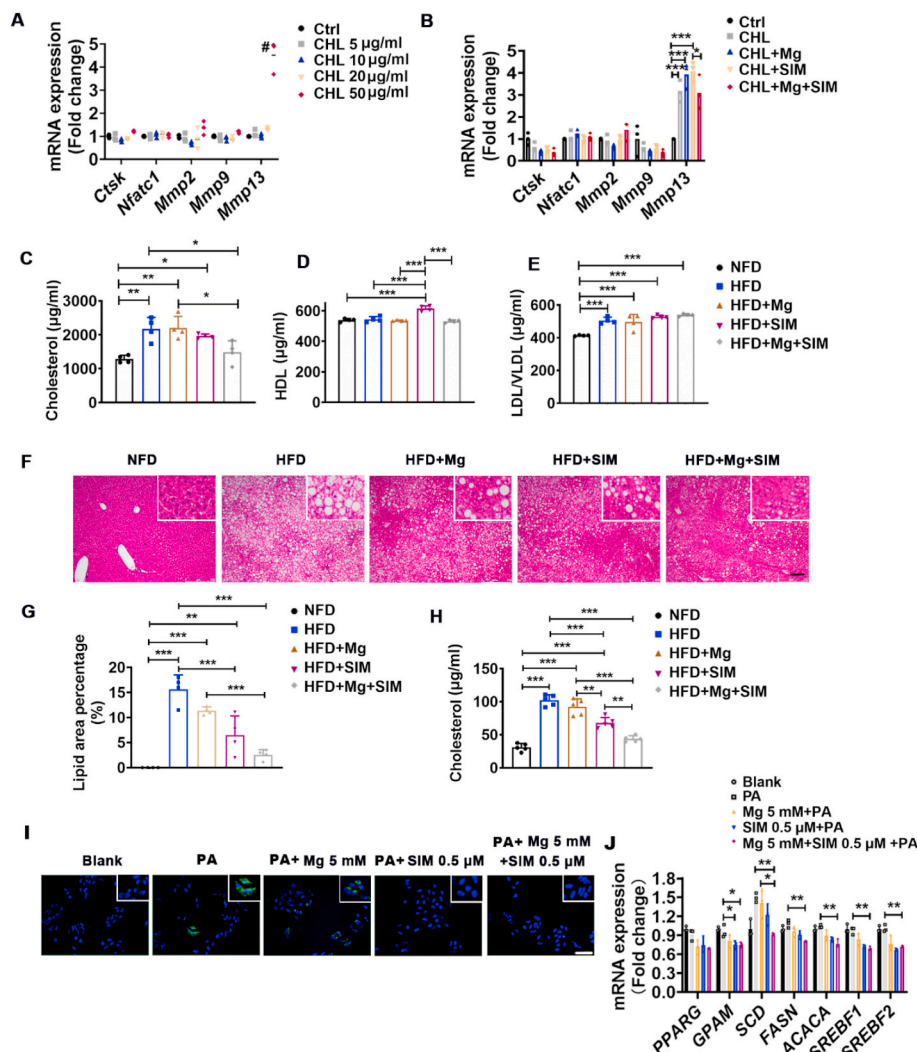
**Fig. 7.** Cholesterol activates the *Mmp13* expression in pre-osteoclasts, but the combined therapy compromises the cholesterol synthesis in hepatocytes.

(A) Relative expression of *Ctsk, Nfatc1, Mmp2, Mmp9,* and *Mmp13* in BMDMs after osteoclastogenic induction for 4 days and following the treatment of cholesterol (CHL) for 12 h (*n* = 3). (B) Relative expression of *Ctsk, Nfatc1, Mmp2, Mmp9,* and *Mmp13* in BMDMs after osteoclastogenic induction for 4 days and following the treatment of mixed cholesterol (50 µg/ml) with Mg (5 mM), SIM (0.5 µM), or 5 mM Mg + 0.5 µM SIM for 12 h (*n* = 3). (C–E) The levels of serum cholesterol (C), HDL (D), and LDL/VLDL (E) at the late-stage therapy (*n* = 4). (F, G) Representative H&E staining and quantification (*n* = 4) of lipid area in liver at the late-stage therapy (The top right corner is a magnification, Scale bar: 250 µm). (H) Cholesterol level of liver lysates at the late-stage therapy (*n* = 5). (I) Representative BODIPY staining of neutral lipids in HepG2 cells pre-treated by Mg, SIM, or Mg + SIM for 1 day and following palmitic acid (0.4 mM) treatment for another 1 day (The top right corner is a magnification; Scale bar: 100 µm). (J) Relative expression of *PPARG, GPAM, SCD, FASN, ACACA, SREBF1,* and *SREBF2* in HepG2 cells pre-treated by Mg, SIM, or Mg + SIM for 1 day and following palmitic acid (0.4 mM) treatment for another 1 day (*n* = 3). All data were presented as mean ± SD. \**P* < 0.05; \*\**P* < 0.01; \*\*\**P* < 0.001; by one-way ANOVA with *Tukey's post hoc* test (A and J); by two-way ANOVA with *Sidak's post hoc* test (B, C, D, E, G, and H).
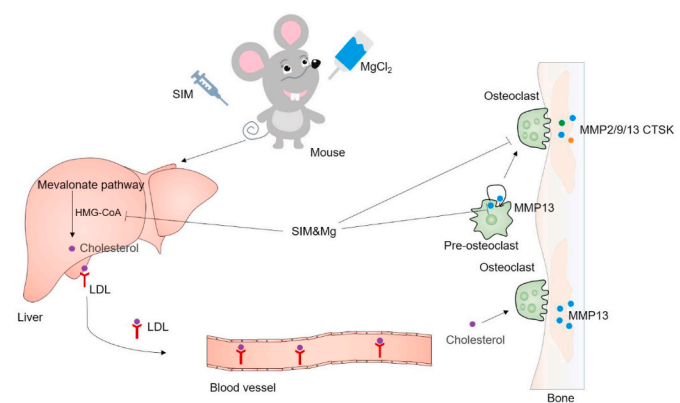


**Fig. 8.** Illustration of the underlying mechanism of combined therapy of Mg²⁺ and SIM that leads to a synergistic effect on attenuating the HFD-induced bone loss via impairing osteoclast maturation and bone resorption in bone marrow. Meanwhile, the combination can directly limit the hepatocytic synthesis of cholesterol.

lipids in the extracellular fluid, making the fats available to cells for the endocytosis, whereas HDL is negatively correlated with the high loading condition of cholesterol [67]. The classical LDL particle function facilitates cholesterol release from liver and transports it to the circulatory

system [67]. The HDL particle definitely functions as the efflux capacity of carrying free cholesterol from cells and delivering cholesteryl esters to various tissues, especially the liver where cholesterol is processed for excretion through the bile [67]. However, we do not find pharmaceutical effects on the adjustment of LDL/VLDL and HDL, indicating the negligible influence on the comprehensive transportation and utilization of cholesterol in the body. Both *in vivo* and *in vitro* experimental results demonstrate the blocked synthesis of cholesterol in hepatocytes under the combination of Mg²⁺ and SIM.

Given the numerous biomolecules regulated by the mevalonate pathway, it comes with a little surprise for the usage of statins experiencing a beneficial effect on prevention or treatment of osteoporosis and bone fracture, in addition to its known effect on limiting hypercholesterolemia [8]. Statins can particularly intervene in the process of bone turnover and remodeling via producing effects on bone resident cells, such as BMSCs and osteoclasts [68]. We fail to find the osteogenic feature of SIM *in vitro*. However, our results corroborate that SIM substantially inhibits the osteoclast formation and activities, and further arrests the synthesis of matrix degrading enzyme in osteoclast under the combined treatments. SIM exerts the inhibitory effect on the MMP release via a post-transcriptional mechanism, and this effect is reversed by mevalonate and geranylgeranyl-pyrophosphate [69]. We find that the BMDMs treated with high dosage of SIM (1 µM) increases the *Mmp13* expression under the osteoclastogenic induction *in vitro*. This result partly explains that SIM increases the risk of trigger finger and shoulder

tendinopathy, possibly correlated with the increased MMP13 release [70]. We thus choose the low dosage of SIM (0.5 μM) to limit the osteoclasts activity by inhibiting the *Ctsk* and *Mmp2/9* expression and avoiding the enhanced *Mmp13* expression *in vitro*. The dosage *in vivo* of SIM (20 mg/kg/day) is also lower as compared with other investigation [71].

In our study, we acquire a desirable result with a physiologically safe concentration of $Mg^{2+}$, which is substantially lower than that in other investigation [36]. Supplementary $Mg^{2+}$ could directly reach bone resident cells and hepatocytes from circulation. Namely, studies should inevitably focus on the effects of $Mg^{2+}$ on these types of cells. Actually, the circulatory system is less sensitive to reflect the scarcity of $Mg^{2+}$ due to the reservoir of $Mg^{2+}$ in bone tissue [72]. About 60% of total $Mg^{2+}$ is stored in the bone. One third of skeletal $Mg^{2+}$ resides on cortical bone either on the surface of hydroxyapatite or in the hydration shell around the crystal [61]. Then the level of $Mg^{2+}$ in serum may be kept constant despite of bone loss at trabecular dominant skeletal sites. Therefore, the time point of supplementary $Mg^{2+}$ for the early-stage therapy (at week 8 of HFD) is earlier than the initial time point of decreased concentration of $Mg^{2+}$ (at week 16 of HFD). We select saline as the matched group to avoid the interference of $Cl^-$ from $MgCl_2$. Moreover, the $Mg^{2+}$-evoked currents are not affected with deletion of external sodium by substitution with choline or replacement of chloride with nitrate [73]. Niflumic acid, a $Cl^-$ channel antagonist, does not alter $Mg^{2+}$ currents, indicating that extracellular $Cl^-$ has no influence on the transport of $Mg^{2+}$ [73]. Besides, both *in vitro* and *in vivo* results demonstrate that the high mineralization is realized with a concentration of 0.8 mM $Mg^{2+}$, which is consistent with previous study [37].

Due to lesser density in trabecular bone as compared with cortical bone, trabecular bone provides only about 20% of the bone mass, but it is predominantly responsible for the dynamic bone turnover (34). We find that the bone loss mainly occurs at trabecular bone in the stage (within 16 weeks of HFD), but the cortical bone becomes more and more porous in following stage (later than 16 weeks post HFD). These results are in line with the fact that the higher expression of Wnt/β-catenin signaling is mainly distributed in trabecular bone and therefore more easily regulated by this signaling than cortical bone under a HFD-fed condition [74,75]. Most studies confirm the independent correlation between HFD and cortical bone mass [76,77]. In the current study, we find the significantly increased cortical porosity and decreased cortical thickness in HFD-fed mice at week 24. Our follow-up time point is longer than other studies, suggesting that the duration of HFD may be crucial for investigating the alteration of cortical bone mass.

Nevertheless, some uncertainties do still exist in our study. Firstly, we have not fully explored the mechanisms of combined therapy on the regulations of hepatocytic metabolism and the synthesis of matrix degrading enzyme in osteoclasts. Secondly, it is now well established that combined therapy could improve the bone mass through two ways, however, their exact contributions remain unclear. Thirdly, our study is not able to eliminate the effect of free cholesterol on osteogenesis. Notwithstanding these limitations, this study does suggest the synergistic effects on lowering cholesterol and improving bone mass in HFD-fed mice.

## 5. Conclusion

Our study demonstrates that combination of $Mg^{2+}$ and SIM leads to a synergistic effect on attenuating the HFD-induced bone loss via impairing osteoclast formation and activities. This study provides a new avenue for clinical translation of statin combined with $Mg^{2+}$ to ameliorate obesity-related bone loss.

## CRediT authorship contribution statement

**Bingyang Dai:** Conceptualization, Methodology, Formal analysis, Investigation, Data curation, Writing - original draft, Software,

Validation. **Xu Li:** Conceptualization, Methodology, Formal analysis, Data curation, Writing - original draft, Software, Validation. **Jiankun Xu:** Conceptualization, Methodology, Investigation, Funding acquisition, Writing - original draft, Software, Validation. **Yuwei Zhu:** Methodology, Formal analysis, Data curation. **Le Huang:** Methodology, Formal analysis, Data curation. **Wenxue Tong:** Methodology, Formal analysis, Data curation. **Hao Yao:** Methodology, Formal analysis, Data curation. **Dick Ho-kiu Chow:** Methodology, Formal analysis, Data curation. **Ling Qin:** Supervision, Writing - review & editing, Data curation, Project administration, Funding acquisition.

## Appendix A. Supplementary data

Supplementary data to this article can be found online at https://doi.org/10.1016/j.bioactmat.2021.01.027.

## Declaration of competing interest

The authors declare that they have no known competing financial interests or personal relationships that could have appeared to influence the work reported in this paper.

## References

[1] R.H. Eckel, S.M. Grundy, P.Z. Zimmet, The metabolic syndrome, Lancet (London, England) 365 (9468) (2005) 1415–1428.

[2] H.M. Lakka, D.E. Laaksonen, T.A. Lakka, L.K. Niskanen, E. Kumpusalo, J. Tuomilehto, J.T. Salonen, The metabolic syndrome and total and cardiovascular disease mortality in middle-aged men, Jama 288 (21) (2002) 2709–2716.

[3] S. Malik, N.D. Wong, S.S. Franklin, T.V. Kamath, G.J. L'Italien, J.R. Pio, G. R. Williams, Impact of the metabolic syndrome on mortality from coronary heart disease, cardiovascular disease, and all causes in United States adults, Circulation 110 (10) (2004) 1245–1250.

[4] W.S. Browner, D.G. Seeley, T.M. Vogt, S.R. Cummings, Non-trauma mortality in elderly women with low bone mineral density. Study of Osteoporotic Fractures Research Group, Lancet (London, England) 338 (8763) (1991) 355–358.

[5] D.M. Kado, W.S. Browner, T. Blackwell, R. Gore, S.R. Cummings, Rate of bone loss is associated with mortality in older women: a prospective study, J. Bone Miner. Res. : the official journal of the American Society for Bone and Mineral Research 15 (10) (2000) 1974–1980.

[6] P. von der Recke, M.A. Hansen, C. Hassager, The association between low bone mass at the menopause and cardiovascular mortality, Am. J. Med. 106 (3) (1999) 273–278.

[7] S. Lapmanee, N. Charoenphandhu, R. Aeimlapa, P. Suntornsaratoon, K. Wongdee, W. Tiyasatkulkovit, K. Kengkoom, K. Chaimongkolnukul, D. Seriwatanachai, N. Krishnamra, High dietary cholesterol masks type 2 diabetes-induced osteopenia and changes in bone microstructure in rats, Lipids 49 (10) (2014) 975–986.

[8] C.C. Mandal, High cholesterol deteriorates bone Health: new insights into molecular mechanisms, Front. Endocrinol. 6 (2015) 165.

[9] B. Dai, Q. Li, X. Song, Y. Ge, J. Wu, K. Zhang, C. Wang, Y. Zhang, H. Teng, C. Li, Q. Jiang, Knockdown of Ggps1 in chondrocyte expedites fracture healing by accelerating the progression of endochondral ossification in mice, J. Bone Miner. Metabol. 36 (2) (2018) 133–147.

[10] J. Zheng, M.J. Brion, J.P. Kemp, N.M. Warrington, M.C. Borges, G. Hemani, T. G. Richardson, H. Rasheed, Z. Qiao, P. Haycock, M. Ala-Korpela, G. Davey Smith, J. H. Tobias, D.M. Evans, The effect of plasma lipids and lipid-lowering interventions on bone mineral density: a mendelian randomization study, J. Bone Miner. Res. : the official journal of the American Society for Bone and Mineral Research 35 (7) (2020) 1224–1235.

[11] T. Fukui, M. Ii, T. Shoji, T. Matsumoto, Y. Mifune, Y. Kawakami, H. Akimaru, A. Kawamoto, T. Kuroda, T. Saito, Y. Tabata, R. Kuroda, M. Kurosaka, T. Asahara, Therapeutic effect of local administration of low-dose simvastatin-conjugated gelatin hydrogel for fracture healing, J. Bone Miner. Res. : the official journal of the American Society for Bone and Mineral Research 27 (5) (2012) 1118–1131.

[12] G. Mundy, R. Garrett, S. Harris, J. Chan, D. Chen, G. Rossini, B. Boyce, M. Zhao, G. Gutierrez, Stimulation of bone formation in vitro and in rodents by statins, Science (New York, N.Y.) 286 (5446) (1999) 1946–1949.

[13] D.J. Norman, D.R. Illingworth, J. Munson, J. Hosenpud, Myolysis and acute renal failure in a heart-transplant recipient receiving lovastatin, N. Engl. J. Med. 318 (1) (1988) 46–47.

[14] J. Armitage, The safety of statins in clinical practice, Lancet (London, England) 370 (9601) (2007) 1781–1790.

[15] C.B. Newman, D. Preiss, J.A. Tobert, T.A. Jacobson, R.L. Page 2nd, L.B. Goldstein, C. Chin, L.R. Tannock, M. Miller, G. Raghuveer, P.B. Duell, E.A. Brinton, A. Pollak, L.T. Braun, F.K. Welty, Statin safety and associated adverse events: a scientific statement from the American heart association, Arterioscler. Thromb. Vasc. Biol. 39 (2) (2019) e38–e81.

[16] D.I. Swerdlow, D. Preiss, K.B. Kuchenbaecker, M.V. Holmes, J.E. Engmann, T. Shah, R. Sofat, S. Stender, P.C. Johnson, R.A. Scott, M. Leusink, N. Verweij, S. J. Sharp, Y. Guo, C. Giambartolomei, C. Chung, A. Peasey, A. Amuzu, K. Li, J. Palmen, P. Howard, J.A. Cooper, F. Drenos, Y.R. Li, G. Lowe, J. Gallacher, M. C. Stewart, I. Tzoulaki, S.G. Buxbaum, A.D. van der, N.G. Forouhi, N.C. Onland-Moret, Y.T. van der Schouw, R.B. Schnabel, J.A. Hubacek, R. Kubinova, M. Baceviciene, A. Tamosiunas, A. Pajak, R. Topor-Madry, U. Stepaniak, S. Malyutina, D. Baldassarre, B. Sennblad, E. Tremoli, U. de Faire, F. Veglia, I. Ford, J.W. Jukema, R.G. Westendorp, G.J. de Borst, P.A. de Jong, A. Algra, W. Spiering, A.H. Maitland-van der Zee, O.H. Klungel, A. de Boer, P.A. Doevendans, C.B. Eaton, J.G. Robinson, D. Duggan, J. Kjekshus, J.R. Downs, A.M. Gotto, A.C. Keech, R. Marchioli, G. Tognoni, P.S. Sever, N.R. Poulter, D.D. Waters, T.R. Pedersen, P. Amarenco, H. Nakamura, J.J. McMurray, J.D. Lewsey, D.I. Chasman, P. M. Ridker, A.P. Maggioni, L. Tavazzi, K.K. Ray, S.R. Seshasai, J.E. Manson, J. F. Price, P.H. Whincup, R.W. Morris, D.A. Lawlor, G.D. Smith, Y. Ben-Shlomo, P. J. Schreiner, M. Fornage, D.S. Siscovick, M. Cushman, M. Kumari, N.J. Wareham, W.M. Verschuren, S. Redline, S.R. Patel, J.C. Whittaker, A. Hamsten, J.A. Delaney, C. Dale, T.R. Gaunt, A. Wong, D. Kuh, R. Hardy, S. Kathiresan, B.A. Castillo, P. van der Harst, E.J. Brunner, A. Tybjaerg-Hansen, M.G. Marmot, R.M. Krauss, M. Tsai, J. Coresh, R.C. Hoogeveen, B.M. Psaty, L.A. Lange, H. Hakonarson, F. Dudbridge, S. E. Humphries, P.J. Talmud, M. Kivimäki, N.J. Timpson, C. Langenberg, F. W. Asselbergs, M. Voevoda, M. Bobak, H. Pikhart, J.G. Wilson, A.P. Reiner, B. J. Keating, A.D. Hingorani, N. Sattar, HMG-coenzyme A reductase inhibition, type 2 diabetes, and bodyweight: evidence from genetic analysis and randomised trials, Lancet (London, England) 385 (9965) (2015) 351–361.

[17] P. Amarenco, J. Labreuche, Lipid management in the prevention of stroke: review and updated meta-analysis of statins for stroke prevention, the Lancet, Neurology 8 (5) (2009) 453–463.

[18] A. Rosanoff, M.S. Seelig, Comparison of mechanism and functional effects of magnesium and statin pharmaceuticals, J. Am. Coll. Nutr. 23 (5) (2004) 501s–505s.

[19] G.C. Ness, C.D. Spindler, G.A. Benton, Characteristics of magnesium-adenosine triphosphate-dependent inactivators of 3-hydroxy-3-methylglutaryl coenzyme A reductase, J. Biol. Chem. 255 (19) (1980) 9013–9016.

[20] B.T. Altura, M. Brust, S. Bloom, R.L. Barbour, J.G. Stempak, B.M. Altura, Magnesium dietary intake modulates blood lipid levels and atherogenesis, Proc. Natl. Acad. Sci. U.S.A. 87 (5) (1990) 1840–1844.

[21] B.C.T. Kieboom, S. Ligthart, A. Dehghan, S. Kurstjens, J.H.F. de Baaij, O.H. Franco, A. Hofman, R. Zietse, B.H. Stricker, E.J. Hoorn, Serum magnesium and the risk of prediabetes: a population-based cohort study, Diabetologia 60 (5) (2017) 843–853.

[22] S. Kurstjens, J.H. de Baaij, H. Bouras, R.J. Bindels, C.J. Tack, J.G. Hoenderop, Determinants of hypomagnesemia in patients with type 2 diabetes mellitus, Eur. J. Endocrinol. 176 (1) (2017) 11–19.

[23] F. Guerrero-Romero, A. Flores-García, S. Saldaña-Guerrero, L.E. Simental-Mendía, M. Rodríguez-Morán, Obesity and hypomagnesemia, Eur. J. Intern. Med. 34 (2016) 29–33.

[24] X. Feng, J.M. McDonald, Disorders of bone remodeling, Annual review of pathology 6 (2011) 121–145.

[25] Y.T. Tsao, Y.Y. Shih, Y.A. Liu, Y.S. Liu, O.K. Lee, Knockdown of SLC41A1 magnesium transporter promotes mineralization and attenuates magnesium inhibition during osteogenesis of mesenchymal stromal cells, Stem Cell Res. Ther. 8 (1) (2017) 39.

[26] Y. Zhang, J. Xu, Y.C. Ruan, M.K. Yu, M. O'Laughlin, H. Wise, D. Chen, L. Tian, D. Shi, J. Wang, S. Chen, J.Q. Feng, D.H. Chow, X. Xie, L. Zheng, L. Huang, S. Huang, K. Leung, N. Lu, L. Zhao, H. Li, D. Zhao, X. Guo, K. Chan, F. Witte, H. C. Chan, Y. Zheng, L. Qin, Implant-derived magnesium induces local neuronal production of CGRP to improve bone-fracture healing in rats, Nat. Med. 22 (10) (2016) 1160–1169.

[27] M.M. Belluci, T. Schoenmaker, C. Rossa-Junior, S.R. Orrico, T.J. de Vries, V. Everts, Magnesium deficiency results in an increased formation of osteoclasts, J. Nutr. Biochem. 24 (8) (2013) 1488–1498.

[28] D. Maradze, D. Musson, Y. Zheng, J. Cornish, M. Lewis, Y. Liu, High magnesium corrosion rate has an effect on osteoclast and mesenchymal stem cell role during bone remodelling, Sci. Rep. 8 (1) (2018) 10003.

[29] N. Ghosh-Choudhury, C.C. Mandal, G.G. Choudhury, Statin-induced Ras activation integrates the phosphatidylinositol 3-kinase signal to Akt and MAPK for bone morphogenetic protein-2 expression in osteoblast differentiation, J. Biol. Chem. 282 (7) (2007) 4983–4993.

[30] C.J. Edwards, T.D. Spector, Statins as modulators of bone formation, Arthritis Res. 4 (3) (2002) 151–153.

[31] X. Xu, A. Grijalva, A. Skowronski, M. van Eijk, M.J. Serlie, A.W. Ferrante Jr., Obesity activates a program of lysosomal-dependent lipid metabolism in adipose tissue macrophages independently of classic activation, Cell Metabol. 18 (6) (2013) 816–830.

[32] S.P. Parihar, R. Guler, D.M. Lang, H. Suzuki, A.D. Marais, F. Brombacher, Simvastatin enhances protection against Listeria monocytogenes infection in mice by counteracting Listeria-induced phagosomal escape, PloS One 8 (9) (2013), e75490.

[33] A.P. Owens 3rd, F.H. Passam, S. Antoniak, S.M. Marshall, A.L. McDaniel, L. Rudel, J.C. Williams, B.K. Hubbard, J.A. Dutton, J. Wang, P.S. Tobias, L.K. Curtiss, A. Daugherty, D. Kirchhofer, J.P. Luyendyk, P.M. Moriarty, S. Nagarajan, B. C. Furie, B. Furie, D.G. Johns, R.E. Temel, N. Mackman, Monocyte tissue factor-dependent activation of coagulation in hypercholesterolemic mice and monkeys is inhibited by simvastatin, J. Clin. Invest. 122 (2) (2012) 558–568.

[34] I. Institute of Medicine Standing Committee on the Scientific Evaluation of Dietary Reference, The National Academies Collection: Reports Funded by National Institutes of Health, Dietary Reference Intakes for Calcium, Phosphorus, Magnesium, Vitamin D, and Fluoride, National Academies Press (US) Copyright ©, National Academy of Sciences., Washington (DC), 1997, 1997.

[35] M. de Lordes Lima, T. Cruz, J.C. Pousada, L.E. Rodrigues, K. Barbosa, V. Canguçu, The effect of magnesium supplementation in increasing doses on the control of type 2 diabetes, Diabetes Care 21 (5) (1998) 682–686.

[36] H.B. Ravn, T.L. Korsholm, E. Falk, Oral magnesium supplementation induces favorable antiatherogenic changes in ApoE-deficient mice, Arterioscler. Thromb. Vasc. Biol. 21 (5) (2001) 858–862.

[37] L.Z. Zheng, J.L. Wang, J.K. Xu, X.T. Zhang, B.Y. Liu, L. Huang, R. Zhang, H.Y. Zu, X. He, J. Mi, Q.Q. Pang, X.L. Wang, Y.C. Ruan, D.W. Zhao, L. Qin, Magnesium and vitamin C supplementation attenuates steroid-associated osteonecrosis in a rat model, Biomaterials 238 (2020) 119828.

[38] P. Chavassieux, R. Chapurlat, N. Portero-Muzy, J.P. Roux, P. Garcia, J.P. Brown, C. Libanati, R.W. Boyce, A. Wang, A. Grauer, Bone-forming and antiresorptive effects of romosozumab in postmenopausal women with osteoporosis: bone histomorphometry and microcomputed tomography analysis after 2 and 12 Months of treatment, J. Bone Miner. Res. : the official journal of the American Society for Bone and Mineral Research 34 (9) (2019) 1597–1608.

[39] D.W. Dempster, J.E. Compston, M.K. Drezner, F.H. Glorieux, J.A. Kanis, H. Malluche, P.J. Meunier, S.M. Ott, R.R. Recker, A.M. Parfitt, Standardized nomenclature, symbols, and units for bone histomorphometry: a 2012 update of the report of the ASBMR Histomorphometry Nomenclature Committee, J. Bone Miner. Res. : the official journal of the American Society for Bone and Mineral Research 28 (1) (2013) 2–17.

[40] M.L. Bouxsein, S.K. Boyd, B.A. Christiansen, R.E. Guldberg, K.J. Jepsen, R. Müller, Guidelines for assessment of bone microstructure in rodents using micro-computed tomography, J. Bone Miner. Res. : the official journal of the American Society for Bone and Mineral Research 25 (7) (2010) 1468–1486.

[41] L.F. Liu, W.J. Shen, M. Ueno, S. Patel, S. Azhar, F.B. Kraemer, Age-related modulation of the effects of obesity on gene expression profiles of mouse bone marrow and epididymal adipocytes, PloS One 8 (8) (2013), e72367.

[42] X. Dou, X. Wei, G. Liu, S. Wang, Y. Lv, J. Li, Z. Ma, G. Zheng, Y. Wang, M. Hu, W. Yu, D. Zhao, Effect of porous tantalum on promoting the osteogenic differentiation of bone marrow mesenchymal stem cells in vitro through the MAPK/ERK signal pathway, J Orthop Translat 19 (2019) 81–93.

[43] B. Wei, C. Jin, Y. Xu, X. Du, C. Yan, C. Tang, M. Ansari, L. Wang, Chondrogenic differentiation of marrow clots after microfracture with BMSC-derived ECM scaffold in vitro, Tissue engineering, Part. Accel. 20 (19–20) (2014) 2646–2655.

[44] Y. Indo, S. Takeshita, K.A. Ishii, T. Hoshii, H. Aburatani, A. Hirao, K. Ikeda, Metabolic regulation of osteoclast differentiation and function, J. Bone Miner. Res. : the official journal of the American Society for Bone and Mineral Research 28 (11) (2013) 2392–2399.

[45] S. Joshi-Barve, S.S. Barve, K. Amancherla, L. Gobejishvili, D. Hill, M. Cave, P. Hote, C.J. McClain, Palmitic acid induces production of proinflammatory cytokine interleukin-8 from hepatocytes, Hepatology (Baltimore, Md 46 (3) (2007) 823–830.

[46] W. Li, J. Yu, Y. Liu, X. Huang, N. Abumaria, Y. Zhu, X. Huang, W. Xiong, C. Ren, X. G. Liu, D. Chui, G. Liu, Elevation of brain magnesium prevents synaptic loss and reverses cognitive deficits in Alzheimer's disease mouse model, Mol. Brain 7 (2014) 65.

[47] T. Jämsä, P. Jalovaara, Z. Peng, H.K. Väänänen, J. Tuukkanen, Comparison of three-point bending test and peripheral quantitative computed tomography analysis in the evaluation of the strength of mouse femur and tibia, Bone 23 (2) (1998) 155–161.

[48] Y. Kong, W. Feng, X. Zhao, P. Zhang, S. Li, Z. Li, Y. Lin, B. Liang, C. Li, W. Wang, H. Huang, Statins ameliorate cholesterol-induced inflammation and improve AQP2 expression by inhibiting NLRP3 activation in the kidney, Theranostics 10 (23) (2020) 10415–10433.

[49] W.L. Miller, H.S. Bose, Early steps in steroidogenesis: intracellular cholesterol trafficking, J. Lipid Res. 52 (12) (2011) 2111–2135.

[50] K.R. Feingold, C. Grunfeld, Introduction to lipids and lipoproteins, in: K. R. Feingold, B. Anawalt, A. Boyce, G. Chrousos, K. Dungan, A. Grossman, J. M. Hershman, G. Kaltsas, C. Koch, P. Kopp, M. Korbonits, R. McLachlan, J. E. Morley, M. New, L. Perreault, J. Purnell, R. Rebar, F. Singer, D.L. Trence, A. Vinik, D.P. Wilson (Eds.), Endotext, MDText.Com, Inc. Copyright © 2000-2020, MDText.com, Inc., South Dartmouth (MA), 2000.

[51] J.K. Liao, U. Laufs, Pleiotropic effects of statins, Annu. Rev. Pharmacol. Toxicol. 45 (2005) 89–118.

[52] M. Tencerova, F. Figeac, N. Ditzel, H. Taipaleenmaki, T.K. Nielsen, M. Kassem, High-fat diet-induced obesity promotes expansion of bone marrow adipose tissue and impairs skeletal stem cell functions in mice, J. Bone Miner. Res. : the official journal of the American Society for Bone and Mineral Research 33 (6) (2018) 1154–1165.

[53] S.A. Shapses, D. Sukumar, Bone metabolism in obesity and weight loss, Annu. Rev. Nutr. 32 (2012) 287–309.

[54] L. Chen, J.J.Y. Zheng, G. Li, J. Yuan, J.R. Ebert, H. Li, J. Papadimitriou, Q. Wang, D. Wood, C.W. Jones, M. Zheng, Pathogenesis and clinical management of obesity-

related knee osteoarthritis: impact of mechanical loading, Journal of orthopaedic translation 24 (2020) 66–75.

[55] Y.H. Hsu, S.A. Venners, H.A. Terwedow, Y. Feng, T. Niu, Z. Li, N. Laird, J.D. Brain, S.R. Cummings, M.L. Bouxsein, C.J. Rosen, X. Xu, Relation of body composition, fat mass, and serum lipids to osteoporotic fractures and bone mineral density in Chinese men and women, Am. J. Clin. Nutr. 83 (1) (2006) 146–154.

[56] P. Szulc, A. Varennes, P.D. Delmas, J. Goudable, R. Chapurlat, Men with metabolic syndrome have lower bone mineral density but lower fracture risk–the MINOS study, J. Bone Miner. Res. : the official journal of the American Society for Bone and Mineral Research 25 (6) (2010) 1446–1454.

[57] E.S. Ramos-Junior, G.A. Leite, C.C. Carmo-Silva, T.M. Taira, K.B. Neves, D. F. Colón, L.A. da Silva, S.L. Salvador, R.C. Tostes, F.Q. Cunha, S.Y. Fukada, Adipokine chemerin bridges metabolic dyslipidemia and alveolar bone loss in mice, J. Bone Miner Research 32 (5) (2017) 974–984.

[58] F. Parhami, Y. Tintut, W.G. Beamer, N. Gharavi, W. Goodman, L.L. Demer, Atherogenic high-fat diet reduces bone mineralization in mice, J. Bone Miner. Res. : the official journal of the American Society for Bone and Mineral Research 16 (1) (2001) 182–188.

[59] E. Istvan, Statin inhibition of HMG-CoA reductase: a 3-dimensional view, Atherosclerosis Suppl. 4 (1) (2003) 3–8.

[60] U. Gröber, J. Schmidt, K. Kisters, Magnesium in prevention and therapy, Nutrients 7 (9) (2015) 8199–8226.

[61] W. Jahnen-Dechent, M. Ketteler, Magnesium basics, Clinical kidney journal 5 (Suppl 1) (2012) i3–i14.

[62] P.D. Thompson, G. Panza, A. Zaleski, B. Taylor, Statin-associated side effects, J. Am. Coll. Cardiol. 67 (20) (2016) 2395–2410.

[63] F.S. Sarr, Y.C. Guillaume, C. André, Magnesium cation effect on passive diffusion of statin molecules: molecular chromatography approach, J. Pharmaceut. Biomed. Anal. 47 (3) (2008) 651–657.

[64] A. Hruby, J.B. Meigs, C.J. O'Donnell, P.F. Jacques, N.M. McKeown, Higher magnesium intake reduces risk of impaired glucose and insulin metabolism and progression from prediabetes to diabetes in middle-aged americans, Diabetes Care 37 (2) (2014) 419–427.

[65] F. Guerrero-Romero, R.A. Rascón-Pacheco, M. Rodríguez-Morán, J.E. de la Peña, N. Wacher, Hypomagnesaemia and risk for metabolic glucose disorders: a 10-year follow-up study, Eur. J. Clin. Invest. 38 (6) (2008) 389–396.

[66] J. Bertinato, C. Wu Xiao, W.M. Ratnayake, L. Fernandez, C. Lavergne, C. Wood, E. Swist, Lower serum magnesium concentration is associated with diabetes,

insulin resistance, and obesity in South Asian and white Canadian women but not men, Food Nutr. Res. 59 (2015) 25974.

[67] E.A. Ivanova, V.A. Myasoedova, A.A. Melnichenko, A.V. Grechko, A.N. Orekhov, Small Dense Low-Density Lipoprotein as Biomarker for Atherosclerotic Diseases, Oxidative Medicine and Cellular Longevity 2017, 2017, p. 1273042.

[68] S.R. Shah, C.A. Werlang, F.K. Kasper, A.G. Mikos, Novel applications of statins for bone regeneration, National science review 2 (1) (2015) 85–99.

[69] M. Massaro, A. Zampolli, E. Scoditti, M.A. Carluccio, C. Storelli, A. Distante, R. De Caterina, Statins inhibit cyclooxygenase-2 and matrix metalloproteinase-9 in human endothelial cells: anti-angiogenic actions possibly contributing to plaque stability, Cardiovasc. Res. 86 (2) (2010) 311–320.

[70] I. Marie, H. Delafenêtre, N. Massy, C. Thuillez, C. Noblet, Tendinous disorders attributed to statins: a study on ninety-six spontaneous reports in the period 1990-2005 and review of the literature, Arthritis Rheum. 59 (3) (2008) 367–372.

[71] L. Li, D. Cao, H. Kim, R. Lester, K. Fukuchi, Simvastatin enhances learning and memory independent of amyloid load in mice, Ann. Neurol. 60 (6) (2006) 729–739.

[72] S. Castiglioni, A. Cazzaniga, W. Albisetti, J.A. Maier, Magnesium and osteoporosis: current state of knowledge and future research directions, Nutrients 5 (8) (2013) 3022–3033.

[73] A. Goytain, G.A. Quamme, Identification and characterization of a novel mammalian Mg2+ transporter with channel-like properties, BMC Genom. 6 (2005) 48.

[74] H.M. Penrose, S. Heller, C. Cable, H. Nakhoul, M. Baddoo, E. Flemington, S. E. Crawford, S.D. Savkovic, High-fat diet induced leptin and Wnt expression: RNA-sequencing and pathway analysis of mouse colonic tissue and tumors, Carcinogenesis 38 (3) (2017) 302–311.

[75] J. Li, Q. Bao, S. Chen, H. Liu, J. Feng, H. Qin, A. Li, D. Liu, Y. Shen, Y. Zhao, Z. Zong, Different bone remodeling levels of trabecular and cortical bone in response to changes in Wnt/β-catenin signaling in mice, J. Orthop. Res. : official publication of the Orthopaedic Research Society 35 (4) (2017) 812–819.

[76] C.R. Doucette, M.C. Horowitz, R. Berry, O.A. MacDougald, R. Anunciado-Koza, R. A. Koza, C.J. Rosen, A high fat diet increases bone marrow adipose tissue (MAT) but does not alter trabecular or cortical bone mass in C57BL/6J mice, J. Cell. Physiol. 230 (9) (2015) 2032–2037.

[77] J.J. Cao, B.R. Gregoire, H. Gao, High-fat diet decreases cancellous bone mass but has no effect on cortical bone mass in the tibia in mice, Bone 44 (6) (2009) 1097–1104.